

Effect of Silicon Nitride/Oxide on the Structure and the Thermal Conductivity of CoSi Nanocomposites

Maria Ioannou¹, Andreas Delimitis², Elli Symeou¹, John Giapintzakis¹, and Theodora Kyratsi^{1,*}

¹Department of Mechanical and Manufacturing Engineering, University of Cyprus, 1678 Nicosia, Cyprus

²CPERI/CERTH, 6th km. Charilaou-Thermis Road, 57001 Thermi, Thessaloniki, Greece

In this work, the fabrication of nanocomposites with silicon nitride/oxide into the thermoelectric matrix of cobalt silicide is presented. The different concentrations of nano-Si₃N₄ were intentionally introduced by mechanical grinding while it was found that the nanocomposites also included SiO₂ phase at micro- as well as at nano-scale. The structural and morphological modifications of the materials were studied by powder X-ray Diffraction, Scanning Electron Microscopy and Transmission Electron Microscopy. The nanocomposites were studied in terms of Hall Effect, Seebeck coefficient, electrical and thermal conductivity. Emphasis is given on the lattice thermal conductivity that was analyzed based on Effective Medium Theory and the contribution of each phase is taken into account.

Keywords: Thermoelectricity, CoSi, Nanocomposite, Nano-Si₃N₄, Nano-SiO₂, Thermal Conductivity, Effective Medium Theory, Porosity.

1. INTRODUCTION

In recent years, the development of thermoelectric (TE) materials for energy conversion applications made significant progress.¹ Thermoelectric figure of merit, ZT, is related to the thermal conductivity (κ), electrical conductivity (σ) and Seebeck coefficient (S) at certain temperatures (T) via the relationship: $ZT = S^2\sigma T/\kappa$. The main contributors to the thermal conductivity are phonons and charge carriers (electrons and holes). The overall thermal conductivity (κ_{total}) of a material is defined as:² $\kappa_{\text{total}} = \kappa_{\text{lattice}} + \kappa_{\text{electron}}$, where κ_{lattice} is the lattice thermal conductivity and κ_{electron} is the electronic contribution.

Different approaches has been applied, aiming the reduction of lattice thermal conductivity, with nanostructuring of bulk materials being recently the main effort in most systems. The development of TE nanocomposites, produced by adding nano-inclusions or mixing particles of nanostructured phases, have been reported for increased phonon scattering.^{3–6} Several types of nano-inclusions or nano-particles^{7,8} such as semiconductors, metals, semimetals and ceramics including nanowires,⁹ carbon nanotubes¹⁰ or fullerenes¹¹ have been introduced in a variety of TE materials. The lattice thermal conductivity

of the nanocomposite samples was suppressed because of the significantly increased number of grain boundaries that effectively scatter phonons. The effect of grain size has been recently studied in several papers [12–18] reporting the changes on the thermal conductivity with nanoscale grain size while details of phonon transport mechanisms are still not very well understood.¹⁹

Among silicides, CoSi has been reported as a promising material for thermoelectrics,^{20–23} This material shows very high electrical conductivity but quite large Seebeck coefficient at room temperature,^{24,25} therefore, its thermoelectric power factor ($S^2\sigma$) is high (order of $\mu\text{WK}^{-2}\text{cm}^{-1}$) and comparable to that of state-of-the-art Bi₂Te₃ materials.²⁶ However, ZT is not high mainly due to its high thermal conductivity, therefore, this work focuses more on this parameter. The reduction of the lattice thermal conductivity was attempted via the fabrication of nanocomposites.

According to the author's best knowledge, there is very limited work²⁷ on the development of CoSi nanocomposite materials aiming to decrease its high thermal conductivity. In Ref. [27], the introduction of SiO₂ and Al₂O₃ was attempted and the reduction of the thermal conductivity was successful. In this work, the inclusion of nano-Si₃N₄ is studied as a non-oxide alternative. The nanoparticles of silicon nitride were intentionally introduced

* Author to whom correspondence should be addressed.

at different concentrations as a secondary phase in the cobalt silicide matrix to produce nanocomposites. Moreover, nano-SiO₂ was also unintentionally formed as third phase in the nanocomposites. The materials were studied in terms of structural and morphological characteristics. The thermoelectric properties (Hall Effect, Seebeck coefficient, electrical conductivity, thermal conductivity and figure of merit) are also discussed. Finally, the reduction of lattice thermal conductivity via formation of nanocomposite materials is discussed in the view of Effective Medium Theory.

2. MATERIALS AND METHODS

2.1. Reagents

Chemicals in this work were used as obtained:

- (i) Cobalt powder (-22 mesh [= 622 μm], 99.998% purity, Alfa Aesar);
- (ii) Silicon powder (crystalline, +100 mesh [= 149 μm], 99.9% purity, Alfa Aesar) and
- (iii) Silicon Nitride (Si₃N₄) nanopowder (<50 nm, ≥98.5% purity, Sigma-Aldrich). All manipulations were carried out under argon in a dry glove box.

2.2. Grinding and Heating Treatment

The cobalt and silicon powders were mixed in the 1:1 ratio, ground in a mortar and cold-pressed to pellets. The pellets were placed in Al₂O₃ crucibles, sealed in silica tubes under vacuum, heated at 1000 °C for 20 hrs and ground again.

The prepared CoSi powders were mixed with nano-Si₃N₄ following (1 - x) CoSi + xSi₃N₄ for x values 0.0%, 1.0%, 2.5%, 5.0%, 7.5% and 10% (referred in text as CoSi/xSi₃N₄). After mixing, the powders were hot-pressed at 1000 °C for 60 min under 80 MPa pressure and argon flow (in HP20 system from Thermal Technologies Inc.) in order to perform thermoelectric measurements. The hot-pressed nanocomposite pellets had densities between 4.65 to 6.25 g/cm³. The density of the hot-pressed CoSi matrix corresponds to ~95% of the theoretical value for the CoSi and reduces to the ~75% for the material with 10%Si₃N₄. The experimental density of the pellets (ρ_{EXP}) was found from mass (m) and volume (V) measurements using the equation

$$\rho_{\text{EXP}} = m/V \quad (1)$$

While the theoretical density of the composites was estimated based on the equation:

$$\rho_{\text{TH}} = f_{\text{CoSi}}\rho_{\text{CoSi}} + f_{\text{Si}_3\text{N}_4}\rho_{\text{Si}_3\text{N}_4} \quad (2)$$

where *f* and *ρ* is the fraction and the density of the individual phases. The porosity of the pellets was then estimated based on (ρ_{TH} - ρ_{EXP})/ρ_{TH}.

2.3. Structural Characterization and Elemental Analysis

Powder X-ray diffraction (PXRD) patterns were obtained on all materials, using a Rigaku Miniflex system with Ni-filtered Cu Kα radiations (30 kV, 15 mA) in order to identify the phases and evaluate purity of the products. The morphological characterization of the powders was carried out by scanning electron microscopy (SEM) (Tescan Vega LSU as well as Jeol 840 A). The EDX mapping was performed in a JEOL scanning electron microscope (JSM-6610LV) and a Bruker Energy Dispersive X-ray spectrometer (QUANTAX 200). Conventional and high resolution transmission electron microscopy (TEM, HRTEM) observations were carried out on selected samples using a JEOL 2011 TEM operating at 200 kV with a point resolution of 0.23 nm and fitted with an EDX detector (Oxford Instruments, model INCA x-sight). Samples suitable for electron microscopy were prepared by dispersing crushed material on ultrathin lacey C films supported on 3.05 mm copper grids.

2.4. Thermoelectric Properties

2.4.1. Hall Effect

The measurements were carried out based on Van der Pauw configuration at room temperature using magnetic field of 2 T in the Quantum Design—Physical Property Measurement System (PPMS).

2.4.2. Seebeck Coefficient and Electrical Conductivity

The measurements were carried out on the hot-pressed pellets simultaneously using a commercial ZEM-3 seebeck coefficient and electrical resistivity measurement system from ULVAC-RIKO. Data were recorded in the temperature range of room temperature to 973 K. The measurements were performed under a residual pressure of helium gas to facilitate good thermal contact.

2.4.3. Thermal Conductivity

A Netzsch LFA-457 system was used to measure thermal diffusivity and heat capacity of the hot-pressed pellets. The thermal conductivity was calculated from the experimental thermal diffusivity (α) and a specific heat capacity data (C_p), as well as density values (ρ), based on the equation κ = α × ρ × C_p. The C_p values were obtained from measurements using the same laser flash equipment using pyroceramic material as reference.

3. RESULTS AND DISCUSSION

3.1. Structural Characterization and Nanocomposite Fabrication

CoSi is the only existing phase in the powder that was mixed with Si₃N₄ to prepare the composites, see Figure 1. After mixing the two materials (CoSi and Si₃N₄) and hot

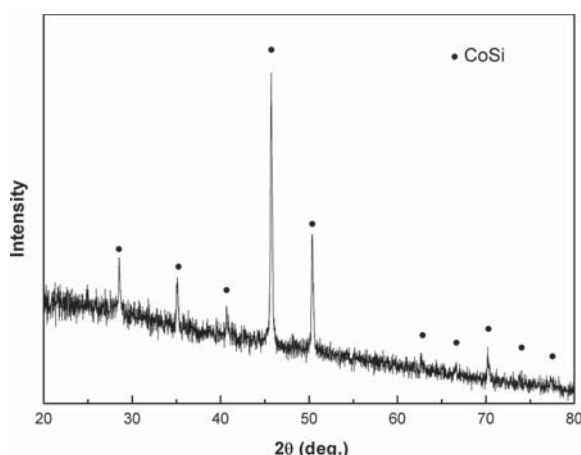


Figure 1. Powder X-ray diffraction pattern for CoSi powder used for the fabrication of CoSi/ x Si₃N₄ pellets.

pressing, the PXRD patterns did not include any additional peaks due to both, strong fluorescence background of the matrix and low Si₃N₄ concentration.

Figure 2 illustrates the density of the hot-pressed CoSi/ x Si₃N₄ pellets as a function of the Si₃N₄ content. The theoretical density of the hot pressed pellets, also shown in Figure 2 as solid line, was expected to decrease from 6.58 g/cm³ to 6.27 g/cm³ with Si₃N₄ concentration up to 10%. On the other hand, the experimental pellet density was found monotonously decreasing from 6.25 g/cm³ to 4.65 g/cm³. It is clear that these values were lower than those expected from Eq. (2) and, additionally, their difference increases with Si₃N₄ concentration. It is obvious that the porosity of the pellets increases reaching 25% (circles in Fig. 2) with the introduction of 10% hard silicon nitride. Hot-pressing at higher temperature (up to 1200 °C) did not further improve the density of the nanocomposites.

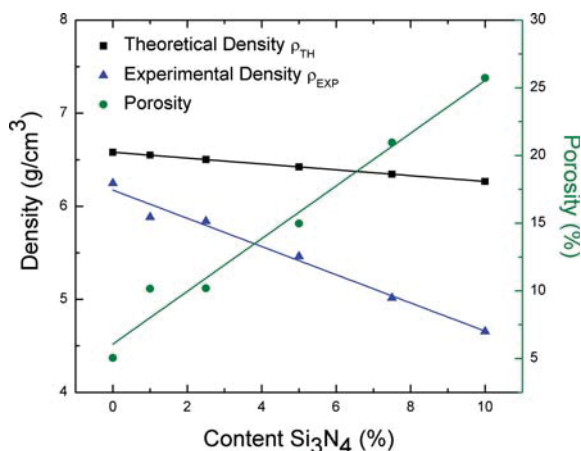


Figure 2. Theoretical density, experimental density and porosity of the hot-pressed CoSi/ x Si₃N₄ nanocomposites pellets as a function of the Si₃N₄ content.

3.2. Electron Microscopy and Elemental Analysis

In order to study the morphology of the CoSi nanocomposites, the hot-pressed samples were examined by SEM/EDX (see Figs. 3–4). Figures 3(a) and 4(a) show the backscattered electron (BSE) images where the grain boundaries on the surface of the CoSi/ x Si₃N₄ pellets were clearly observed.

EDX mapping was used to evaluate the distribution of the elements, i.e., Co, Si, O and N. Figures 3(b–e) and 4(b–e) show the distribution of Co, Si, O and N on CoSi/2.5% Si₃N₄ and CoSi/5.0% Si₃N₄ pellets, respectively. Clearly, the distribution of Co and Si seems more or less uniform. Increased quantity of nitrogen was observed on the grain boundaries and this can be attributed to the Si₃N₄ aggregates at micro-scale in all composites regardless the Si₃N₄ concentration, see Figures 3(e) and 4(e). Interestingly, quantity of oxygen was also observed on the grain boundaries suggesting the formation of SiO₂ phase, probably due to slight oxidation during synthesis/pressing of the pellets (Figs. 3(d) and 4(d)).

The nanocomposites were further studied by TEM observations, as shown in Figure 5 for the sample CoSi/2.5% Si₃N₄. The main CoSi phase consists of large crystals with typical sizes 400–900 nm. They are single crystalline in nature, as shown by the selected area diffraction (SAD) pattern inset in Figure 5(a), where the main CoSi reflections are indexed. Interestingly, along with CoSi, the existence of SiO₂ phase is also observed, agglomerated with the parent grains, as depicted in Figure 5(a). The SiO₂ is entirely amorphous and, thus, is formed into particles with no specific size and morphology. Its presence was confirmed by EDX analysis and a typical spectrum is illustrated as an inset in the same image. Based on the TEM observations, the SiO₂ phase comprises of not more than 5–10% in the samples studied.

Introduction of Si₃N₄ nanoparticles took place between the CoSi grains, as presented in both Figure 5(a) (black arrowed) and the HRTEM image of Figure 5(b). The particle has almost spherical shape with a diameter of 20 nm and is coherently embedded with CoSi, as proved by the Moiré fringe pattern superimposed on the two crystals, CoSi and Si₃N₄. The lattice fringes resolved are attributed to the (20 $\bar{2}$ 1), (11 $\bar{2}$ 0) and (110) crystal planes of hexagonal Si₃N₄ and cubic CoSi, respectively.

Apart from the small Si₃N₄ nanoparticles embedded inside CoSi, the formation of single crystalline Si₃N₄ grains was also detected by TEM and EDX. Such grains are shown in Figure 5(c), in agglomeration with SiO₂ particles, as well. The Si₃N₄ grains are up to 300 nm in size and are single crystalline, as demonstrated by the SAD pattern inset in the figure, where the [11 $\bar{2}$ 0] projection is shown. It has to be noted here that the majority of the Si₃N₄ phase in the sample is in the form of the large crystallites. Moreover, a few Si₃N₄ nanoparticles were also detected inside the SiO₂ amorphous particles, both by HRTEM imaging experiments, as well as by EDX point analysis.

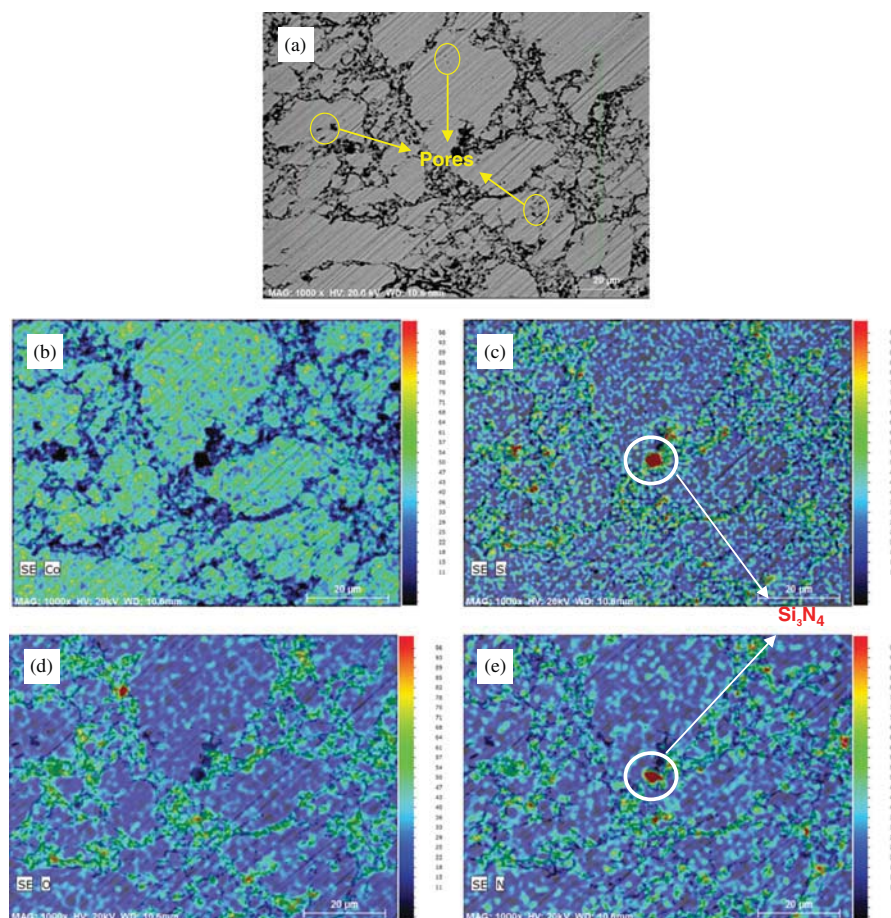


Figure 3. Backscattered electron (BSE) image (a) and the EDX elemental distribution maps (b–e) of Co, Si, O and N, respectively, of the CoSi/2.5% Si_3N_4 nanocomposites. The colors are qualitatively adjusted based on the concentration of each element separately. The coloring scheme follows a rainbow scale, from blue (minimum concentration) to red (maximum concentration) and does not correspond to quantitative results.

3.3. Thermoelectric Properties

Table I lists the results of the measurements (carrier concentration, Seebeck coefficient, electrical and thermal conductivity and mobility) at 300 K for CoSi materials. The sign of the Hall coefficient was negative for all samples, indicating that the conductivity is mainly due to electrons, as expected. The carrier concentration was found in the order of $4\text{--}5 \cdot 10^{20} \text{ cm}^{-3}$ (slightly decrease with x values) suggesting that the incorporation of the Si_3N_4 in the matrix does not really affect them, see Table I. Moreover, the electrical conductivity significantly drops with increased different Si_3N_4 concentration, and this is clearly attributed to the lower mobility, see Figure 6. This significant effect of Si_3N_4 on the reduction of the mobility (factor >3 when 10% Si_3N_4 is added) can be explained based on the contribution of the $\text{Si}_3\text{N}_4/\text{SiO}_2$ aggregates that are formed on the grain boundaries of the materials, as shown by electron microscopy, as well as the contribution of porosity. When porosity exceeds 15%, the mobility reduction is stronger.

Figures 7 and 8 shows the temperature dependence of electrical conductivity (7a), the Seebeck coefficient (7b), thermal conductivity (8a) and the lattice thermal conductivity (8b) of the CoSi hot-pressed pellets. The electrical properties of CoSi indicate semi-metallic behavior in agreement with the literature.^{28–30} Figure 7(b) presents the temperature dependence of Seebeck coefficient of the n -type CoSi members. The Seebeck coefficient values are quite similar for all samples being between $80\text{--}90 \mu\text{V/K}$ at room temperature. The thermal conductivity of CoSi nanocomposites, see Figure 8(a), decreases as a function of temperature showing typical behavior of the TE materials. The room temperature thermal conductivities of CoSi nanocomposites decrease from $15.7 \text{ W/m} \cdot \text{K}$ to $4.2 \text{ W/m} \cdot \text{K}$ when 0.0% and 10.0% Si_3N_4 participates, see Table I. The lattice thermal conductivity (κ_{lattice}) was estimated, aiming to study the effect of the inclusions in the CoSi matrix, using the Wiedemann-Franz relation $\kappa_{\text{lattice}} = \kappa_{\text{total}} - \kappa_{\text{electron}}$, where $\kappa_{\text{electron}} = L \cdot \sigma \cdot T$ with $L = 2.45 \times 10^{-8} \text{ V}^2\text{K}^{-2}$, see Figure 8(b). The lattice thermal

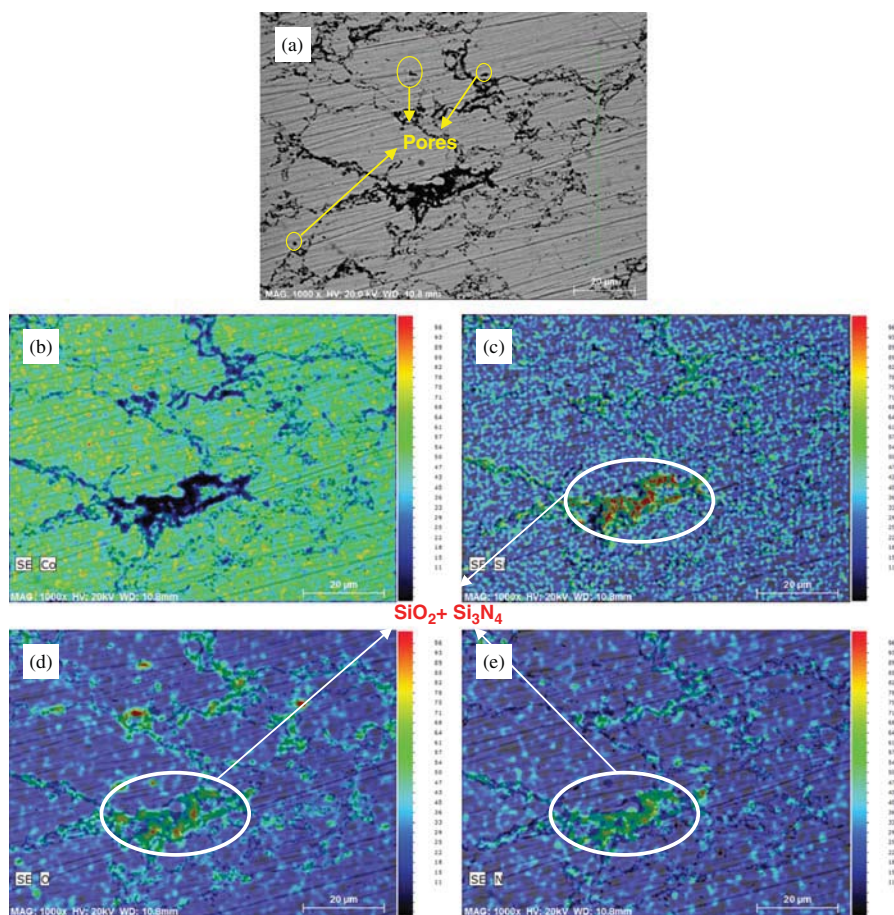


Figure 4. Backscattered electron (BSE) image (a) and the EDX elemental distribution maps (b–e) of Co, Si, O and N, respectively, of the CoSi/5.0% Si₃N₄ nanocomposites. Colors are the same as in Figure 3.

conductivity of all samples showed strong dependence on x values, decreased monotonously with nano-Si₃N₄ concentration and this is discussed in more detail in the next section. Maximum ZT values for each concentration is presented in Table I. The highest value here is 0.19 at 630 K and it is not higher than previous work²⁷ mainly due to the decrease of the mobility. Therefore, more work can be done on the distribution of the different phases and the grain boundaries of the material.

3.4. Analysis of the Lattice Thermal Conductivity

Thermal conductivity in multi-phase systems may be modeled in two ways:

(a) with effective medium theory (EMT), where a property (thermal conductivity) is derived as kind of weighted average of the properties of each individual phase. EMT applies in micro-scale constituents, where each phase is large enough to develop its own properties.

(b) In terms of the semi-classical theoretical calculations of the mechanisms of phonon scattering, based on the modified Callaway model.³¹ In this case, phonon

relaxation time is developed from contributions Umklapp and Normal processes, dislocations, strains, point defects, and precipitates.³² Precipitates have two contributions for short-and long-wavelength scattering.

Opposite to EMT, the relaxation time due to the nanoprecipitates does not depend on the thermal conductivity of the precipitated phase, but only on particle size (short-wavelength scattering) and mass difference (long-wavelength scattering).³³ In this part we will consider the former (EMT) case. The expression:^{34, 35}

$$\sum_i f_i \frac{\kappa_i - \kappa}{\kappa_i + 2\kappa} = 0 \quad \text{and} \quad \sum_i f_i = 1 \quad (3)$$

where κ_i is the thermal conductivity of the i -th phase with volume fraction f_i . Considering the CoSi/Si₃N₄ system, the Eq. (3) was written as:

$$f_{\text{CoSi}} \frac{\kappa_{\text{CoSi}} - \kappa}{\kappa_{\text{CoSi}} + 2\kappa} + f_{\text{Si}_3\text{N}_4} \frac{\kappa_{\text{Si}_3\text{N}_4} - \kappa}{\kappa_{\text{Si}_3\text{N}_4} + 2\kappa} = 0 \quad \text{and} \quad (4)$$

$$f_{\text{CoSi}} + f_{\text{Si}_3\text{N}_4} = 1$$

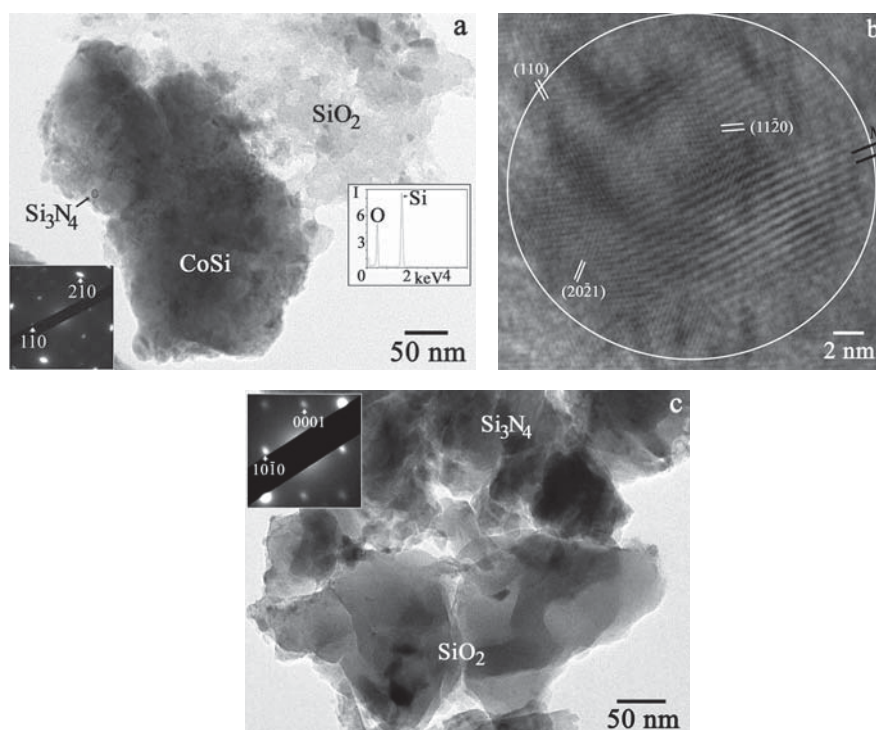


Figure 5. TEM/HRTEM images from the CoSi/2.5% Si_3N_4 nanocomposite sample. (a) TEM image of the main CoSi phase and agglomerated SiO_2 particles. The SAD pattern and EDX spectrum from CoSi and SiO_2 , respectively, are shown as insets in (a); (b) HRTEM image of a characteristic Si_3N_4 nanoparticle inside the CoSi matrix, (c) TEM image of Si_3N_4 crystallites, aggregated with SiO_2 amorphous particles. The SAD pattern inset confirms the crystallinity of the Si_3N_4 phase.

Table I. Thermoelectric properties of CoSi nanocomposites ($0 \leq x \leq 10\%$) at 300 K.

Composition	x (%)	Carrier Concentration n (10^{20}cm^{-3})	Mobility (cm^2/Vs)	Electrical conductivity (S/cm)	Seebeck coefficient ($\mu\text{V}/\text{K}$)	Thermal conductivity ($\text{W}/\text{m}\cdot\text{K}$)	Max ZT @650 K
100.0 CoSi:0.0 Si_3N_4	0.0	5.61	63.79	5732	-80.5	15.7	0.17
99.0 CoSi:1.0 Si_3N_4	1.0	5.11	62.39	5104	-90.4	13.0	0.17
97.5 CoSi:2.5 Si_3N_4	2.5	4.15	56.35	3746	-92.6	10.9	0.19
95.0 CoSi:5.0 Si_3N_4	5.0	4.64	39.05	2902	-85.9	7.6	0.18
92.5 CoSi:7.5 Si_3N_4	7.5	4.28	26.73	1833	-84.6	5.4	0.15
90.0 CoSi:10.0 Si_3N_4	10.0	4.11	19.91	1311	-78.6	4.2	0.12

where f and κ are the fraction and the lattice thermal conductivity of the composites and the f_{CoSi} , $f_{\text{Si}_3\text{N}_4}$ and κ_{CoSi} and $\kappa_{\text{Si}_3\text{N}_4}$ correspond to the constituent phases. The fraction $f_{\text{Si}_3\text{N}_4}$ was ranging in 0.0 to 0.1 while f_{CoSi} was calculated following $f_{\text{CoSi}} + f_{\text{Si}_3\text{N}_4} = 1$, see Table II. Taking into consideration the known fractions, the lattice thermal conductivity of the matrix ($\kappa_{\text{CoSi}} = 13.38 \text{ W}/\text{m}\cdot\text{K}$)^a and the Si_3N_4 ($\kappa_{\text{Si}_3\text{N}_4} = 30.1 \text{ W}/\text{m}\cdot\text{K}$)³⁶, Eq. (4) is solved numerically for the lattice thermal conductivity of the nanocomposites κ . The results of the calculation are

^aThe lattice thermal conductivity of the matrix κ_{CoSi} , was estimated based on an equation similar to Eq. (4) considering 4.7% porosity as presented in Figure 1.

drawn in Figure 9(a) with the upper line labeled “EMT (CoSi/ Si_3N_4).” According to these calculations, the lattice thermal conductivity was predicted to increase from $13.4 \text{ W}/\text{m}\cdot\text{K}$ to about $14.6 \text{ W}/\text{m}\cdot\text{K}$ when 10% Si_3N_4 is incorporated due to the higher thermal conductivity of the nitride phase. However, it is clear that the experimental lattice thermal conductivity of the composite materials is significantly lower than the predicted from EMT (CoSi/ Si_3N_4) and the trend is opposite (decreasing) reaching the value of $3.2 \text{ W}/\text{m}\cdot\text{K}$.

When EMT is applied, in the form of Eq. (4), the contribution of the particles (Si_3N_4) in the CoSi matrix is considered. However, this does not contain the contribution of any interfacial thermal resistance between the two

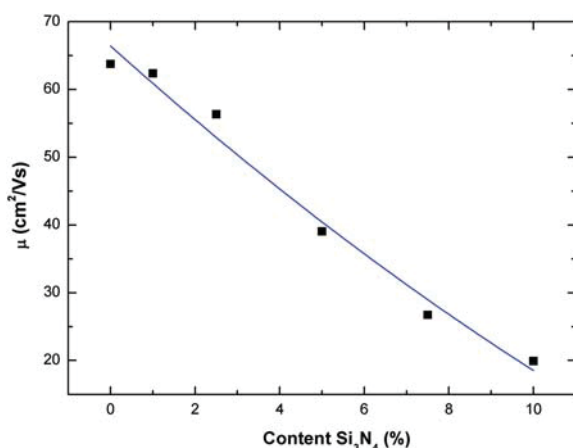


Figure 6. Mobility of the hot-pressed CoSi/ x Si₃N₄ nanocomposites pellets as a function of the Si₃N₄ content.

phases in the composite. In order to evaluate the effect of thermal resistance of the interface between particle and matrix (thickness of d) we applied a methodology that predicts the effective thermal conductivity in terms

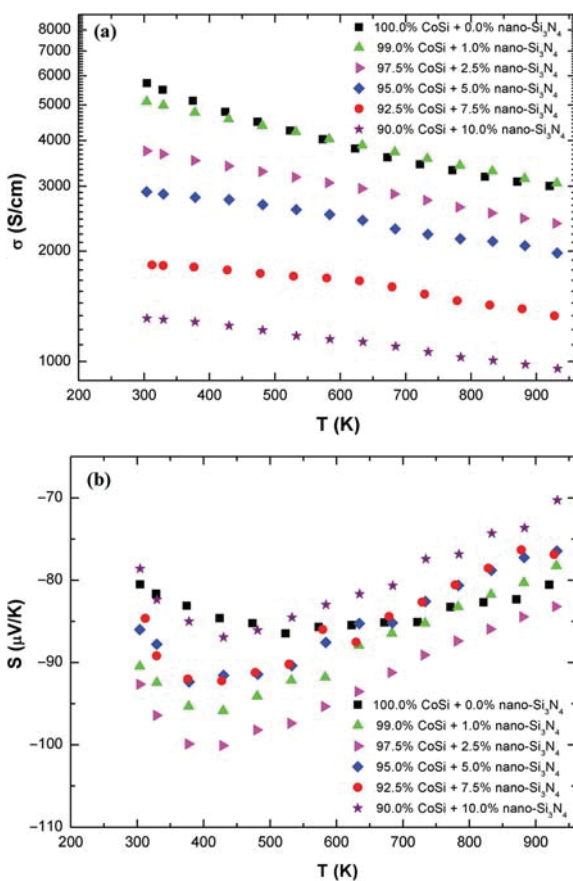


Figure 7. Temperature dependence of electrical conductivity (a) and Seebeck coefficient (b) for hot-pressed CoSi/ x Si₃N₄ nanocomposites pellets.

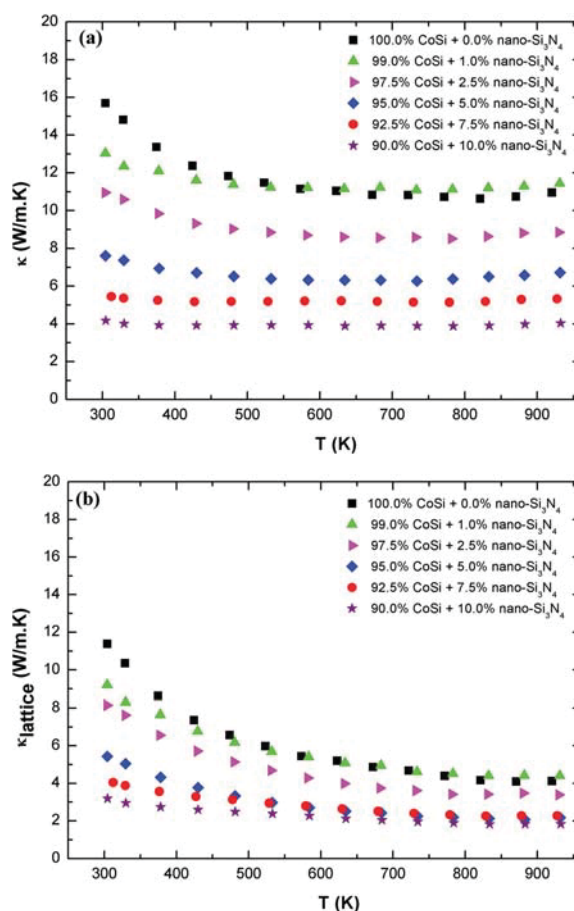


Figure 8. Thermal conductivity (a) and lattice thermal conductivity (b) for hot-pressed CoSi/ x Si₃N₄ nanocomposites pellets.

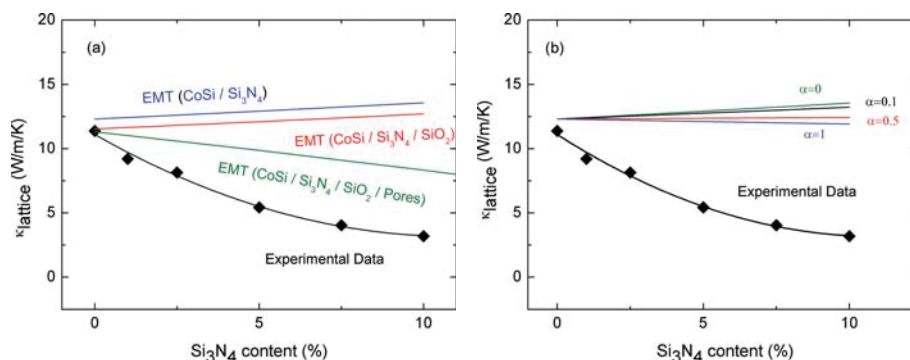
of EMT combined with the essential concept of Kapitza thermal contact resistance.³⁷ For this reason, the following equation³⁴ was used:

$$\begin{aligned} \kappa = & \kappa_{\text{CoSi}} \kappa_{\text{Si}_3\text{N}_4} (1 + 2\alpha) \\ & + 2\kappa_{\text{CoSi}} + 2f_{\text{Si}_3\text{N}_4} [\kappa_{\text{Si}_3\text{N}_4} (1 - \alpha) - \kappa_{\text{CoSi}}] \\ & / \kappa_{\text{Si}_3\text{N}_4} (1 + 2\alpha) + 2\kappa_{\text{CoSi}} \\ & - 2f_{\text{Si}_3\text{N}_4} [\kappa_{\text{Si}_3\text{N}_4} (1 - \alpha) - \kappa_{\text{CoSi}}] \end{aligned} \quad (5)$$

where α is a dimensionless parameter, defined by the ratio α_k/α_1 in which the interfacial thermal resistance is concentrated on a surface of zero thickness and characterized by Kapitza radius, α_k , ($\alpha_k = R_{Bd} \cdot \kappa_{\text{CoSi}}$ with $R_{Bd} = \lim_{\delta \rightarrow 0} (\delta/\kappa_s)$). α_1 is the diameter of the particles and κ_s is the thermal conductivity of the interface. Figure 9(b) shows how the thermal conductivity of the composite material, consisting by CoSi and Si₃N₄ is affected by the interfacial thermal resistance (α values of 0, 0.1, 0.5 and 1.0 were taken). Clearly, increase of the interfacial contribution leads to decrease of the total thermal conductivity

Table II. Fractions and lattice thermal conductivity values used for EMT analysis.

EMT	f_{CoSi}	$f_{\text{Si}_3\text{N}_4}$	f_{SiO_2}	f_{pores}	κ_{CoSi}	$\kappa_{\text{Si}_3\text{N}_4}$	κ_{SiO_2}	κ_{pores}
CoSi/Si ₃ N ₄	$1-f_2$	0–0.1	–	–	13.38	30.1	–	–
CoSi/Si ₃ N ₄ /SiO ₂	$1-f_2-f_3$	0–0.1	0.05	–	13.38	30.1	1.38	–
CoSi/Si ₃ N ₄ /SiO ₂ /Pores	$1-f_2-f_3-f_4$	0–0.1	0.05	see Figure 2	13.38	30.1	1.38	0.0256

**Figure 9.** Room temperature thermal conductivity of the hot-pressed CoSi/ x Si₃N₄ nanocomposites pellets as a function of the Si₃N₄ content with (a) calculations based on the EMT and (b) calculations based on the EMT combined with the concept of Kapitza thermal contact resistance.

of the material, however, the reduction is not that significant compare to our data.

Therefore, an additional mechanism was required to be included to the analysis to understand the results. Since electron microscopy studies showed the existence of SiO₂ in the materials, three terms were taken into account in Eq. (3) and the EMT (CoSi/Si₃N₄/SiO₂) model was developed. In this case, the fraction of Si₃N₄ was ranging from 0.0 to 0.1; the fraction of SiO₂ was estimated by electron microscopy and for the purposes of the EMT analysis was kept constant in 0.05; the fraction of CoSi was calculated by the formula $f_{\text{CoSi}} + f_{\text{Si}_3\text{N}_4} + f_{\text{SiO}_2} = 1$, see Table II. Taking into consideration the known volume fractions, the thermal conductivities (Table II), the EMT equation is solved for the nanocomposite thermal conductivity κ . The results of calculation are added in the Figure 9(a) with the line labeled EMT (CoSi/Si₃N₄/SiO₂). Obviously, the predicted values from EMT (CoSi/Si₃N₄/SiO₂) are still much higher than the experimental data.

In addition, the contribution of the porosity on the reduction of the lattice thermal conductivity in these materials cannot be excluded since it is expected to have significant effect. EMT formula was modified to include also the pores of the pellets as fourth term (CoSi/Si₃N₄/SiO₂/Pores). The fractions f were considered based on Table II. Taking into consideration the known volume fractions, the thermal conductivities used previously (Table II), as well as the thermal conductivity of the air ($\kappa_{\text{pores}} = 0.0256$ W/m·K), the nanocomposite thermal conductivity was calculated. The results are included in the Figure 9(a) with the green solid line labeled EMT (CoSi/Si₃N₄/SiO₂/Pores). According to the calculations, the lattice thermal conductivity was predicted to reduce,

however, although the similar trend, it is clear that the experimental lattice thermal conductivity of the composite materials is still lower than the predicted one. Additional interfacial thermal resistance would further decrease the predicted values, but still not as low as the experimental data. At this stage, the lower values can be attributed on the existence of nano-phases in the materials (as observed by electron microscopy) as well as other mechanisms such as the existence of dislocations, point defects and other microstructure elements, as discussed elsewhere^{33,38} that cannot be included in the EMT.

4. CONCLUSION

In conclusion, CoSi nanocomposites materials have been synthesized using CoSi as matrix and nano-Si₃N₄ via solid state reactions, mechanical mixing and hot pressing. Electron microscopy confirmed the existence of nano-Si₃N₄ that were intentionally introduced in the nanocomposites as well as the existence of micro-Si₃N₄ due to agglomeration. Interestingly, the existence of nano- and micro-SiO₂ due to low oxidation of the material during processing was also observed. The thermoelectric properties were significantly affected by the Si₃N₄ and SiO₂ inclusions as well as the pores through the significant decrease of the mobility. The thermal conductivity was strongly affected and was found to decrease with increasing Si₃N₄ concentration. This was attributed to the additional phonon scattering mechanism that is introduced through not only the inclusion of Si₃N₄ but also the existence of SiO₂ and pores. The reduction of lattice thermal conductivity via the formation of nanocomposite materials is discussed in the view of Effective Medium Theory. Three

different cases of this model were studied for reaching of the reduction of lattice thermal conductivity, taking into account the following combinations: CoSi/Si₃N₄, CoSi/Si₃N₄/SiO₂ and CoSi/Si₃N₄/SiO₂/Pores. The experimental data were found to be closer to the results of the EMT (CoSi/Si₃N₄/SiO₂/Pores) although not fully described. Moreover, the contribution of interfacial thermal resistance between the Si₃N₄ nanoparticles is not excluded. The experimental values were still lower than those predicted and this can be attributed to the existence of nano-phases as well as other microstructure elements such as dislocations, point defects etc. More work can be done to optimize the processing conditions, to enhance the nano-effect on the lattice thermal conductivity through improved dispersion that could positively affect the overall figure of merit.

Acknowledgments: This work is part of the Si-THERM Project supported by the Cyprus Research Promotion Foundation's Framework Programme for Research, Technological Development and Innovation 2009–2010 (DESMI 2009–2010), co-funded by the Republic of Cyprus and the European Regional Development Fund and specially under grant PENEK/0311/07. EDX mapping was done on equipment supported by funding from the European Regional Development Fund and the Republic of Cyprus, through the Research Promotion Foundation (Project normal/0308/17).

References and Notes

1. D. M. Rowe, *Thermoelectrics Handbook: Macro to Nano*, CRC Press, Boca Raton, FL (2005).
2. T. M. Tritt, *Thermal Conductivity: Theory, Properties, and Applications*, Kluwer Academic/Plenum Publishers, New York (2005).
3. W. J. Xie, J. He, H. J. Kang, X. F. Tang, S. Zhu, M. Laver, S. Wang, J. R. D. Copley, C. M. Brown, Q. Zhang, and T. M. Tritt, *Nano Lett.* 10, 3283 (2010).
4. E. Alleno, L. Chen, C. Chubilleau, B. Lenoir, O. Roulea, M. F. Trichet, and B. Villeroy, *J. Electron. Mater.* 39, 1966 (2010).
5. M. K. Keshavarz, D. Vasilevskiy, R. A. Masut, and S. Turenne, *J. Electron. Mater.* 42, 1429 (2013).
6. J. L. Mi, X. B. Zhao, T. J. Zhu, and J. P. Tu, *Appl. Phys. Lett.* 91, 172116 (2007).
7. S. F. Fan, J. N. Zhao, Q. Y. Yan, J. Ma, and H. H. Hng, *J. Electron. Mater.* 40, 1018 (2011).
8. H. Lu, P. G. Burke, A. C. Gossard, G. Zeng, A. T. Ramu, J. H. Bahk, and J. E. Bowers, *Adv. Mater.* 23, 2377 (2011).
9. M. Y. Kim, B. K. Yu, and T. S. Oh, *Electron. Mater. Lett.* 8, 269 (2012).
10. D. H. Park, M. Y. Kim, and T. S. Oh, *Curr. Appl. Phys.* 11, S41 (2011).
11. V. A. Kulbachinskii, V. G. Kytin, M. Y. Popov, S. G. Buga, P. B. Stepanov, and V. D. Blank, *J. Solid State Chem.* 193, 64 (2012).
12. T. Takami, M. Horibe, M. Itoh, and J. Cheng, *Phys. Rev. B* 82, 085110 (2010).
13. Y. Kinemuchi, H. Nakano, M. Mikami, K. Kobayashi, K. Watari, and Y. Hotta, *Appl. Phys. Lett.* 108, 053721 (2010).
14. Y. Kinemuchi, M. Mikami, K. Kobayashi, K. Watari, and Y. Hotta, *J. Electron. Mater.* 39, 2059 (2010).
15. J. Lan, Y. H. Lin, Y. Liu, S. Xu, and C. W. Nan, *J. Am. Ceram. Soc.* 95, 2465 (2012).
16. M. Backhaus-Ricoult, J. R. Rustad, D. Vargheese, I. Dutta, and K. Work, *J. Electron. Mater.* 41, 1636 (2012).
17. Y. Wang, K. Fujinami, R. Zhang, C. Wan, N. Wang, Y. Ba, and K. Koumoto, *Appl. Phys. Express* 3, 031101 (2010).
18. A. Jeżowski, J. Mucha, R. Pazik, and W. Strek, *Appl. Phys. Lett.* 90, 114104 (2007).
19. A. J. Minnich, M. S. Dresselhaus, Z. F. Ren, and G. Chen, *Energy Environ. Sci.* 2, 466 (2009).
20. S. Asanabe, D. Shinoda, and Y. Sasaki, *Phys. Rev. A* 134, 774 (1964).
21. G. T. Alekseeva, V. K. Zaitsev, A. V. Petrov, V. I. Tarasov, and M. I. Fedorov, *Sov. Phys. Solid State* 23, 1685 (1981).
22. S. W. Kim, Y. Mishima, and D. C. Choi, *Intermetallics* 10, 177 (2002).
23. K. Maex and M. V. Rossum, *Properties of Metal Silicides*, INSPEC Institute of Engineers, London (1995).
24. W. L. Ren, C. C. Li, L. T. Zhang, K. Ito, and J. S. Wu, *J. Alloys Compd.* 392, 50 (2005).
25. E. Skoug, C. Zhou, Y. Pei, and D. T. Morelli, *Appl. Phys. Lett.* 94, 022115 (2009).
26. R. R. Heikes and R. W. Ure, *Thermoelectricity: Scien. and Engin. Interscience*, New York (1961), p. 427.
27. (a) M. Ioannou, E. Symeou, J. Giapintzakis, and Th. Kyratsi, *J. Electr. Mater.* 43, 3824 (2014); (b) M. Ioannou and Th. Kyratsi, *Research and Reviews in Materials Science and Chemistry* 5, 93 (2015).
28. G. T. Alekseeva, V. K. Zaitsev, A. V. Petrov, V. I. Tarasov, and M. I. Fedorov, *Sov. Phys. Solid State* 23, 1685 (1981).
29. V. K. Zaitsev, M. I. Fedorov, V. I. Tarasov, and A. Adilbekov, *Sov. Phys. Solid State* 19, 996 (1976).
30. V. K. Zaitsev, M. I. Fedorov, S. V. Ordin, and V. I. Tarasov, *Sov. Phys. Solid State* 20, 890 (1978).
31. J. Callaway and H. C. von Baeyer, *Phys. Rev.* 120, 1149 (1960).
32. J. He, L.-D. Zhao, J.-C. Zheng, J. W. Doak, H. Wu, H.-Q. Wang, Y. Lee, C. Wolverton, M. G. Kanatzidis, and V. P. Dravid, *J. Am. Chem. Soc.* 135, 4624 (2013).
33. J. He, S. N. Girard, M. G. Kanatzidis, and V. P. Dravid, *Adv. Funct. Mater.* 20, 764 (2010).
34. V. I. Odelevskii, *J. Tech. Phys.* 21, 667 (1953).
35. R. J. Landauer, *Appl. Phys.* 23, 779 (1952).
36. J. F. Shackelford and W. Alexander, *CRC Materials Science and Engineering Handbook*, CRC Press, Boca Raton, FL (2000).
37. C.-W. Nan, R. Birringer, D. R. Clarke, and H. Gleiter, *J. App. Phys.* 81, 6692 (1997).
38. S.-H. Lo, *Adv. Funct. Mater.* 22, 5175 (2012).

Received: 16 March 2016. Accepted: 10 June 2016.